Quantum simulation and optimization in hot quantum networks

Schuetz, M. J.A.; Vermersch, B.; Kirchmair, G.; Vandersypen, L. M.K.; Cirac, J. I.; Lukin, M. D.; Zoller, P.

DOI
10.1103/PhysRevB.99.241302

Publication date
2019

Document Version
Final published version

Published in
Physical Review B

Rapid Communications

Quantum simulation and optimization in hot quantum networks

M. J. A. Schuetz,[1] B. Vermersch,[2,3] G. Kirchmair,[2,3] L. M. K. Vandersypen,[4] J. I. Cirac,[5] M. D. Lukin,[1] and P. Zoller[2,3]

[1]*Physics Department, Harvard University, Cambridge, Massachusetts 02318, USA*

[2]*Center for Quantum Physics, Institute for Experimental Physics, University of Innsbruck, A-6020 Innsbruck, Austria*

[3]*Institute for Quantum Optics and Quantum Information of the Austrian Academy of Sciences, A-6020 Innsbruck, Austria*

[4]*QuTech and Kavli Institute of NanoScience, TU Delft, 2600 GA Delft, The Netherlands*

[5]*Max-Planck-Institut für Quantenoptik, Hans-Kopfermann-Straße 1, 85748 Garching, Germany*

(Received 13 September 2018; revised manuscript received 18 February 2019; published 27 June 2019)

We propose a setup based on (solid-state) qubits coupled to a common multimode transmission line, which allows for coherent spin-spin interactions over macroscopic on-chip distances, without any ground-state cooling requirements for the data bus. Our approach allows for the realization of fast deterministic nonlocal quantum gates, the simulation of quantum spin models with engineered (long-range) interactions, and provides a flexible architecture for the implementation of quantum approximate optimization algorithms.

DOI: 10.1103/PhysRevB.99.241302

Introduction. One of the leading approaches for scaling up quantum information systems involves a modular architecture that makes use of a combination of short- and long-distance interactions between the qubits [1,2]. In particular, long-distance interactions can be implemented via a quantum bus which can effectively distribute quantum information between remote qubits, as shown in the context of trapped ions [3–7], solid-state systems [8,9], electromechanical resonators [10], as well as circuit QED architectures [11–16]. In this Rapid Communication, we provide a unified theoretical framework for robust distribution of quantum information via a quantum bus that operates at finite temperature [17], fully accounts for the multimode structure of the data bus, and does not require the qubits to be identical. Our approach [cf. Fig. 1(a)] results in an architecture where fully programmable interactions between qubits can be realized in a fast and deterministic way, without any ground-state cooling requirements for the data bus, thereby setting the stage for various applications in the context of quantum information processing [18] in a hot quantum network, different from quantum state transfer discussed previously [19–21]. As illustrated in Fig. 1(b), and discussed in detail below, one can use our scheme to deterministically implement (hot) quantum gates between two qubits. Moreover, we present a recipe to generate a targeted and scalable evolution for a large set of N qubits coupled via a single transmission line, thereby providing a natural architecture for the implementation of quantum algorithms, such as quantum annealing [22] or the quantum approximate optimization algorithm (QAOA) [23–25], designed to find approximate solutions to hard, combinatorial search problems.

The model. We consider a set of qubits $i = 1, 2, \ldots, N$ with corresponding transition frequencies ω_i (typically in the microwave regime) that are coupled to a (multimode) transmission line of length L; compare Fig. 1 for a schematic illustration. The transmission line is described in terms of photonic modes a_n with wave vectors $k_n = n\pi/L$, with a *linear* spectrum $\omega_n = k_n c = n\omega_1$, where $\omega_1 = \pi c/L$ is the frequency of the fundamental mode $n = 1$ and c is the (effective) speed of light. As opposed to transversal (Jaynes-Cummings-like) spin-resonator coupling [26,27], here we focus on *longitudinal* coupling as could be realized (for example) with superconducting qubits [8,28–31] or quantum-dot-based qubits [8,9,32–36]. The Hamiltonian reads ($\hbar = 1$)

$$H_{\rm lab} = \sum_{i=1}^{N} \frac{\omega_i}{2}\sigma_i^z + \sum_{n=1}^{\infty} \omega_n a_n^\dagger a_n + \sum_{i,n} g_{i,n}\sigma_i^z (a_n + a_n^\dagger), \quad (1)$$

with the qubit Pauli matrices $\vec{\sigma}_i$ and $g_{i,n}$ the coupling strength between qubit i and mode n. We show below that for specific times t, which are integer multiples of the round-trip time $t \propto \tau \equiv 2L/c$, the dynamics of the qubits and *all* photons fully decouple, while giving rise to an effective interaction between the qubits.

Analytical solution of time evolution. With the help of the spin-dependent, multimode displacement transformation $U_{\rm pol}^\dagger = \exp[\sum_{n,i} \frac{g_{i,n}}{\omega_n}\sigma_i^z(a_n^\dagger - a_n)]$, in our model the spin dynamics can be decoupled from the resonator dynamics (in the polaron frame), and we find $H_{\rm lab} = U_{\rm pol} H_{\rm pol} U_{\rm pol}^\dagger$, where

$$H_{\rm pol} = \sum_i \frac{\omega_i}{2}\sigma_i^z + \sum_n \omega_n a_n^\dagger a_n + \sum_{i<j} J_{ij}\sigma_i^z\sigma_j^z, \quad (2)$$

with the effective spin-spin interaction

$$J_{ij} = -2\sum_n \frac{g_{i,n}g_{j,n}}{\omega_n}. \quad (3)$$

Therefore, the evolution *in the laboratory frame* reads $e^{-iH_{\rm lab}t} = U_{\rm pol} e^{-iH_{\rm pol}t} U_{\rm pol}^\dagger$, as follows directly from a Taylor expansion and $U_{\rm pol}^\dagger U_{\rm pol} = \mathbb{1}$. Consider now the evolution at stroboscopic times $t_p = p\tau$ (p positive integer), corresponding to multiples of the round-trip time τ. In this case, all the modes *synchronize*, $\exp[-it_p\sum_n \omega_n a_n^\dagger a_n] = \exp[-2\pi i \sum_n n p a_n^\dagger a_n] = \mathbb{1}$, since the number operators $a_n^\dagger a_n$ feature an *integer* spectrum and $\omega_n t_p = 2\pi pn$; thus, the full evolution reduces exactly to $U_{\rm lab}(t_p) = \exp[-iH_{\rm lab}t_p]$,

$$U_{\rm lab}(t_p) = e^{-it_p\sum_i(\omega_i/2)\sigma_i^z} e^{-it_p\sum_{i<j}J_{ij}\sigma_i^z\sigma_j^z}. \quad (4)$$

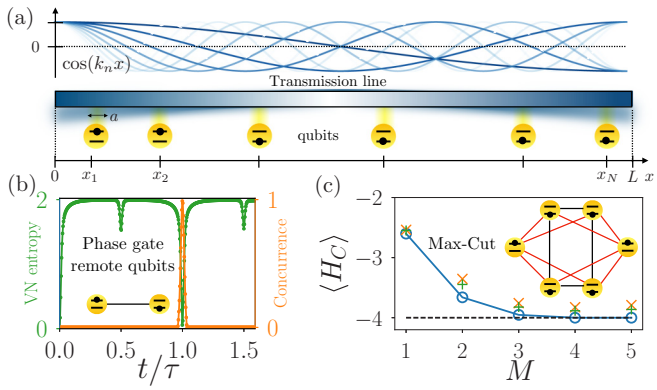

FIG. 1. Hot quantum network. (a) Schematic illustration of N qubits coupled to a transmission line of length L. (b) Dynamic evolution of two qubits, as exemplified for the von Neumann (VN) entropy (left axis) and the concurrence (right axis) of the two-qubit density matrix, with $a = 0.03L$. At the round-trip time $t = \tau$, the qubits fully decouple from the waveguide and form a maximally entangled state, even though the transmission line is far away from the ground state (here, $k_BT = \omega_1$). (c) Quantum approximate optimization algorithm (QAOA) with depth M solving Max-Cut with $N = 6$ qubits and a 4-regular graph (inset), and with decoherence (ideal case: blue; dephasing with rate $\gamma_\phi/J_{\max} = 0.003$: orange; rethermalization with rate $\kappa/|\Delta| = 0.004$: green), and at finite temperature $k_BT = \omega_1$.

Accordingly, for certain times the qubits fully disentangle from the (thermally populated) resonator modes, thereby providing a qubit gate that is insensitive to the state of the resonator, while imposing no conditions on the qubit frequencies ω_i [37]. For specific times, the time evolution in the polaron and the laboratory frame coincide and fully decouple from the photon modes, allowing for the realization of a thermally robust gate, without any need of cooling the transmission line to the vacuum [9]. Moreover, our approach can be straightforwardly combined with standard spin-echo techniques in order to cancel out efficiently low-frequency noise: By synchronizing fast global π rotations with the stroboscopic times t_p, one can enhance the qubit's coherence times from the time-ensemble-averaged dephasing time $T_2^\star$ to the prolonged timescale T_2.

Frequency cutoff. In principle, the spin-spin coupling strength J_{ij} as defined in Eq. (3) involves *all* modes $n = 1, 2, \ldots$, naively leading to unphysical divergencies, as discussed in the context of transversal qubit-resonator coupling in Refs. [38,39]. In any physical implementation, however, there is a microscopic lengthscale a that naturally introduces a frequency cutoff. Specifically, we take the coupling parameters $g_{i,n}$ as $g_{i,n} = g_i\sqrt{n}\int_0^L \cos(k_n x) f(x - x_i)dx$, to account for the fact that the qubits couple to the local voltage, where $f(x - x_i)$ accounts for the microscopic spatial extension of the qubit-transmission line coupling (cf. [40] for details); the factor $\sim\sqrt{n}$ derives from the scaling of the rms zero-point voltage fluctuations with the mode index n, which also implies $g_i \propto L^{-1}$. In the examples below, we will consider for simplicity a box function $f(x) = \delta_{x>0}\delta_{x<a}/a$, leading to $g_{i,n} = g_i\sqrt{n}(\sin[k_n(x_i + a)] - \sin[k_n x_i])/(k_n a)$. Note that if the microscopic lengthscale a is set to zero, the summation over n in Eq. (3) does not converge. Instead for a finite a, and for $|x_i - x_j| > a$ the effective interaction Eq. (3) simplifies to $J_{ij} = g_i g_j/\omega_1$ (cf. [40]). Accordingly, within this exemplary model, the coupling J_{ij} does not depend on a, nor the position of the qubits x_i, and scales as L^{-1}, showing that the time to entangle qubits is only limited by the propagation time τ ($\propto L$) of light through the waveguide.

Applications. We now discuss three applications of our scheme, with a gradual increase in complexity, namely, (i) a *hot* two-qubit phase gate, (ii) the engineering of spin models, and (iii) the implementation of QAOA in the presence of decoherence and finite temperature. To this end, we consider the possibility to potentially boost and fine-tune the effective spin-spin interactions J_{ij} by parametrically modulating the longitudinal spin-resonator coupling, as could be realized with both superconducting qubits [8] or quantum-dot-based qubits [33] (cf. [40] for further details).

Hot phase gate. As a first illustration, we consider the realization of a phase gate between two remote qubits $N = 2$, placed at each edge of the transmission line ($x_1 = 0$, $x_2 = L - a$). Our initial state $\rho_0 = |\Psi_0\rangle\langle\Psi_0| \otimes_n \rho_n$ consists of a pure initial qubit state with $|\Psi_0\rangle = \otimes_j(|0\rangle + i|1\rangle)_j/\sqrt{2}$ and a thermal state of the waveguide with $\rho_n = \exp(-\frac{a_n^\dagger a_n \omega_n}{k_B T})[1 - \exp(-\frac{\omega_n}{k_B T})]$, and we use matrix-product-state (MPS) techniques [42] to show numerically how the hot quantum network generates the desired evolution, Eq. (4). We fix $g_i = \omega_1/\sqrt{8}$ which (under ideal circumstances) leads to a maximally entangled pure state $|\Psi(t_1)\rangle = \exp(-i\frac{\pi}{4}\sigma_1^z\sigma_2^z)|\Psi_0\rangle$ at the gate time $t_g = \pi/(4J_{12})$ after just one round-trip $t_1 = \tau$ (generalizations thereof are provided in [40]). In Fig. 1(b), we show the von-Neumann entropy $\mathcal{E}$ and the concurrence $\mathcal{C}$ of the two-qubit density matrix $\rho_{1,2}$, showing the realization of the gate at $t = t_1$, in the presence of thermal occupation of the waveguide. The corresponding fidelity $\mathcal{F}$ defined as overlap of $\rho_{1,2}$ with respect to the ideal state $|\Psi(t_1)\rangle\langle\Psi(t_1)|$ is shown in Fig. 2(a). In panels (b) and (c) both the mode occupation $\langle a_n^\dagger a_n\rangle$ and the real-space occupation $\langle a_x^\dagger a_x\rangle$ are displayed, with a_x, $0 < x < L$, referring to the discrete sine transform of a_n. In particular, the mode space picture [panel (b)] allows one to visualize the excitation of the linear spectrum of the waveguide, that synchronizes at time $t = \tau$. Conversely, the dynamics in real space [panel (c)] illustrates how qubit-qubit interactions are mediated by photon wave packets propagating ballistically. At the round-trip time $t = \tau$, the waveguide returns to its initial thermal state, as expected. In panel (d), we study the scaling of timing errors by showing the evolution of the error $1 - \mathcal{F}$ around $t \approx t_p$. In the limit of small errors $|\Delta t| \ll (a/c)\sqrt{\omega_1/J_{12}}$, assuming $a \ll L$, the numerical results are well approximated by $1 - \mathcal{F} \approx 4(c/a)^2 J_{12}/\omega_1 \Delta t^2$ (black line), with $\Delta t = t - t_p$. Accordingly, the timing error is sensitive to the cutoff a (as it controls the frequency scale of the couplings), and scales linearly with the effective spin-spin interaction J_{12}, as slower dynamics are less vulnerable to timing inaccuracies $\sim\Delta t$; for further details, in particular related to the influence of temperature on timing errors, and effects due to nonlinear dispersion relations ω_n, cf. [40].

Engineering of spin models. We now extend our discussion to the multiqubit case $N > 2$ and provide a recipe how to generate a targeted and scalable unitary $W = \exp(-i\sum_{i<j} w_{ij}\sigma_i^z\sigma_j^z)$ with desired spin-spin interaction

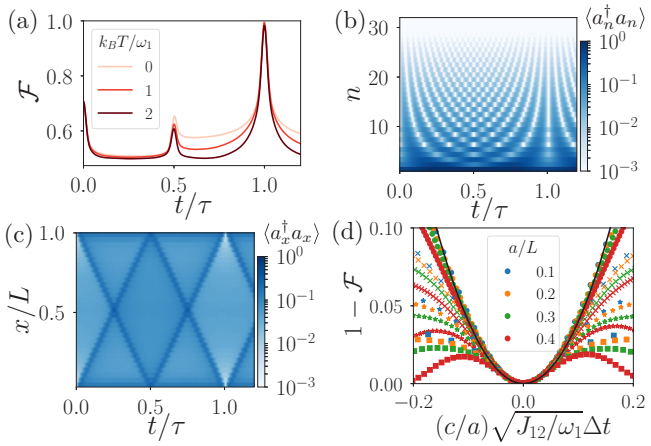

FIG. 2. Hot phase gate between two distant qubits. (a),(b) Fidelity as a function of time τ (a) for $a = 0.03L$ and different transmission line temperatures $0 \leqslant k_BT \leqslant 2\omega_1$. (b) Mode and (c) real-space occupation as a function of the transmission line for $a = 0.03L$ and $k_BT = \omega_1$, with ∼30 modes. (d) Error $1-\mathcal{F}$ around the gate time t_p for $T = 0$ and different values of the cutoff (legend) and number of cycles $p = 1, 4, 8, 16$ (circles, crosses, stars, squares). For small timing errors, all data points collapse to a single curve $4(c/a)^2 J_{12}/\omega_1 \Delta t^2$, shown as a black line.

parameters w_{ij}. To this end, we consider a sequence $q = 1, \ldots, \eta$ of successive cycles where for each stroboscopic cycle (labeled by q) we may apply different coupling amplitudes, i.e., $g_i \to g_i^{(q)}$. For example, this could be done by parametrically modulating the spin-resonator coupling via microwave control [8,33]. The evolution at the end of the sequence is then given by $U_\eta = \exp(-it_p \sum_{i<j} J_{i,j}^{(\eta)} \sigma_i^z \sigma_j^z)$, with $J_{i,j}^{(\eta)} = \sum_{q=1}^{\eta} g_i^{(q)} g_j^{(q)}/\omega_1$, and $t_{\rm run} = \eta t_p$ being the total run time. A straightforward way to generate the desired unitary, i.e., to obtain $w_{ij} = J_{i,j}^{(\eta)} t_p$, consists in diagonalizing the target matrix as $w_{ij} = \sum_{q=1}^{N} w_q u_{i,q} u_{j,q}$ in terms of real eigenvalues w_q and real eigenstates $u_{i,q}$. This leads immediately to the condition $g_i^{(q)} = \sqrt{w_q \omega_1/t_p} u_{i,q}$ to generate exactly W within $\eta = N$ number of cycles, with $t_p \geqslant w_q/J_{\rm max}$, where $J_{\rm max}$ denotes the largest available spin-spin coupling [43]. In other words, we can engineer efficiently arbitrary spin-spin interactions after a time $t_{\rm run} = Nt_p$ which only scales *linearly* with the number of qubits; $t_{\rm run} = 2Nt_p$ in the presence of spin echo. These aspects are illustrated in Fig. 3, where we provide examples for $N = 25$ and both (a) a one-dimensional long-range spin model with power-law decay $w_{ij} = 1/|i-j|^\alpha$ ($\alpha = 1$) and (b) a two-dimensional (2D) model with nearest-neighbor (NN) interactions. The latter demonstrates that our recipe allows for the realization of general spin models in any spatial dimension and geometry (using a simple one-dimensional physical setup). For both models, we observe the progressive emergence of the target spin interaction with increasing values for η, reaching the exact matrix at $\eta = N$. The case of a spin glass with random interactions, and the convergence analysis with respect to η/N are presented in [40].

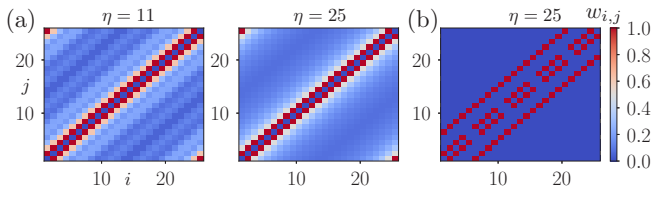

FIG. 3. Engineering of spin models. (a) Long-range interactions $w_{ij} = 1/|i-j|$ and periodic boundary conditions, for $\eta = 11, 25$. (b) 2D nearest-neighbor interactions with open boundary conditions, with $\eta = 25$. Here, the indices i correspond to 2D indices $\mathbf{i} = (i_x, i_y)$ of a square of 5×5 sites using the convention $i = i_x + 5i_y$.

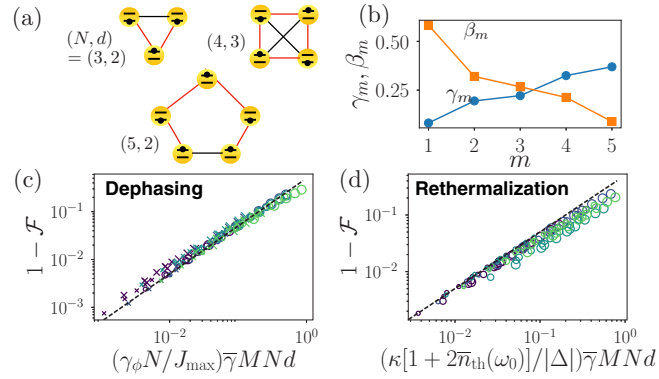

FIG. 4. Simulation of QAOA for Max-Cut, in the presence of decoherence. (a) d-regular graphs with $N = 3, 4, 5$ used for our numerical analysis of decoherence. Our graph with $(N, d) = (6, 4)$ is shown in Fig. 1(c). (b) Optimization parameters γ_m, β_m for $N = 6$, $M = 5$. (c),(d) Scaling of errors with respect to the optimized QAOA wave function $|\boldsymbol{\gamma}, \boldsymbol{\beta}\rangle$ for (c) dephasing and (d) rethermalization. The dashed lines correspond to the scaling expressions given in the text. For each panel, we consider the different graphs, depth $M = 1, 3, 5$, $J_{\rm max}/|\Delta| = 0.02, 0.08$. For (d), we consider $k_BT = 0, \omega_0$. In (c) and (d), the dashed lines represent the curve $y = x/2$.

QAOA. Finally, we show how to generalize the techniques outlined above in order to implement quantum algorithms that provide approximate solutions for hard combinatorial optimization problems such as Max-Cut (cf. Fig. 4 and [40]). As shown in Refs. [23,24], good approximate solutions to these kind of problems can be found by preparing the state $|\boldsymbol{\gamma}, \boldsymbol{\beta}\rangle = U_x(\beta_M) U_{zz}(\gamma_M) \cdots U_x(\beta_1) U_{zz}(\gamma_1) |s\rangle$, with $U_x(\beta_m) = \exp[-i\beta_m \sum_i \sigma_i^x]$, and $U_{zz}(\gamma_m) = \exp[-i\gamma_m H_C]$, where H_C is the cost Hamiltonian encoding the optimization problem, starting initially from a product of σ^x eigenstates, i.e., $|s\rangle = |-, -, \ldots\rangle$, with $|-\rangle = (|0\rangle - |1\rangle)/\sqrt{2}$. In our scheme, this family of states can be prepared by alternating single-qubit operations $U_x(\beta_m)$ with targeted spin-spin interactions generated as described above, with $W \to U_{zz}(\gamma_m)$. Accordingly, for QAOA we repeat our spin-engineering recipe M times with single-qubit rotations interspersed in between. This preparation step is then followed by a measurement in the computational basis, giving a classical string z, with which one can evaluate the objective function $\langle H_C \rangle$ of the underlying combinatorial problem at hand. Repeating this procedure will provide an optimized string z, with the quality of the result improving as the depth of the quantum circuit M is increased [23,24]. To illustrate and verify this approach, we have numerically simulated QAOA with up to $N = 6$ qubits solving Max-Cut for several d-regular graphs with weights

$w_{i,j} = w_{i,j}^{(d)} + d\delta_{i,i}$, as depicted in Figs. 4(a) and 1(c), based on our model Hamiltonian given in Eq. (1), while accounting for both finite temperature and decoherence in the form of qubit dephasing and rethermalization of the resonator mode. While our general multimode setup should (in principle) be well suited for the implementation of QAOA, here (in order to allow for an exact numerical treatment) we consider a simplified single-mode problem (with resonator frequency ω_0), as could be realized using the resonance condition introduced by a monochromatically modulated coupling [8,33]. Specifically, we simulate the Hamiltonian $H = \sum_i (\omega_i/2)\sigma_i^z + \Delta a^\dagger a + \sum_i g_i \sigma_i^z \otimes (a + a^\dagger)$ with controllable couplings g_i [8,33], detuning $\Delta = \omega_0 - \Omega$ and $J_{ij} = -2g_i g_j/\Delta \leqslant J_{\max}$, supplemented by standard dissipators to account for (i) qubit dephasing on a timescale $\sim T_2 = 1/\gamma_\phi$ and (ii) rethermalization of the resonator mode with an effective decay rate $\sim \kappa \bar{n}_{\rm th}(\omega_0)$ [44] (cf. [40] for further details). As demonstrated in Fig. 1(c), for small-scale quantum systems (that are accessible to our exact numerical treatment) our protocol efficiently solves Max-Cut with a circuit depth of $M \lesssim 5$, finding the ground-state energy with very high accuracy (blue curve), corresponding to four *cuts* (shown in red in the inset), even in the presence of moderate noise [compare the cross and plus symbols in Fig. 1(c)].

Decoherence and implementation. Based on our numerical findings and further analytical arguments, we now turn to the eventual limitations imposed by decoherence. Here, we focus on the QAOA protocol, since both our (i) *hot* gate (cf. [40] for a full decoherence-induced error analysis thereof) and (ii) the spin engineering protocol can be viewed as less demanding limits of QAOA, where either M or N (or both) are small, thereby yielding comparatively smaller errors because of a shorter run time; for example, for the two-qubit phase gate $M = 1$, $N = 2$. The total QAOA run time $t_{\rm run}$ can be upper-bounded as $t_{\rm run} \approx \overline{\gamma} MNd/J_{\max}$, with $\overline{\gamma} = 1/M \sum_m \gamma_m$ and the factor $Nd/J_{\max}$ corresponding to the (maximum) time required to implement all eigenvalues $w_q \lesssim d$ of the Max-Cut problem. To keep decoherence effects minimal, this timescale should be shorter than all relevant noise processes. The accumulated dephasing-induced error can be estimated as $\xi_\phi \sim \gamma_\phi N \times \overline{\gamma} MNd/J_{\max}$, where $\sim\gamma_\phi N$ is the effective many-body dephasing rate (cf. [40]); as shown in Fig. 4(c), we have numerically confirmed this scaling for all graphs shown in Figs. 4(a) and 1(c). Similarly, as demonstrated in Fig. 4(d), the indirect rethermalization-induced dephasing error, mediated by incoherent evolution of the resonator mode, can be quantified as $\xi_\kappa \sim \kappa_{\rm eff} \times \overline{\gamma} MNd/|\Delta|$, with total linewidth $\kappa_{\rm eff} = \kappa[2\bar{n}_{\rm th}(\omega_0) + 1]$. The total decoherence-induced error $\xi = \xi_\phi + \xi_\kappa$ can then be optimized with respect to Δ, yielding the compact expression $\xi \approx \overline{\gamma} dMN^{3/2}/\sqrt{C}$, with the cooperativity $C = g^2/(\gamma_\phi \kappa_{\rm eff})$. With this expression, we can bound the maximum number of qubits N and circuit depth M for a given physical setup with cooperativity C.

Specifically, our scheme could be implemented based on superconducting qubits or quantum-dot-based qubits coupled by a common high-quality transmission line, with details given in [40]. For concreteness, let us consider quantum-dot-based qubits [9,33–36] where longitudinal coupling could be modulated via both the detuning [33] or interdot tunneling parameter [34], respectively. With projected two-qubit gate times of $\sim$10 ns [33,34], a coherence time of $T_2 \approx 10$ ms [46,47], and $\omega_0/2\pi \approx 1$ GHz with quality factor $Q \sim 10^6$ [48–50], we estimate decoherence errors to be small ($\lesssim$3%) for up to $N \approx 50$ qubits and a QAOA circuit depth of $M \approx 10$ for a graph with $d \approx 4$, respectively, even in the presence of nonzero thermal occupation with $\bar{n}_{\rm th}(\omega_0) \approx 3$. Further, the performance will be affected by timing errors, as is the case for any gate implementation. However, commercial equipment allows experiments with timing jitter of only a few picoseconds [40,51]. A similar analysis can be made for superconducting qubits [40]. Note that these estimates might be very conservative, as the essential figure of merit in QAOA is not the quantum state fidelity $\mathcal{F}$ but the probability to find the optimal (classical) bit-string z in a sample of projective measurements $\{z_1, z_2, \dots\}$ (obtained after many repetitions of the experiments).

Conclusion. To conclude, we have presented a protocol to generate fast, coherent, long-distance coupling between solid-state qubits, without any ground-state cooling requirements. While this approach has direct applications in terms of the engineering of spin models (e.g., to implement QAOA) it would be interesting to further develop our theoretical treatment in order to increase the level of robustness of our scheme, e.g., to apply protocols based on error correcting photonic codes [54], which can protect against photon losses or rethermalization. Yet another interesting research direction would be to adapt our scheme to other physical setups, say solid-state defect centers coupled by phonons [10].

Acknowledgments. We thank S. Harvey, H. Pichler, P. Scarlino, D. Vasilyev, S. Wang, and L. Zhou for fruitful discussions. Numerical simulations were performed using the ITensor library [55] and QuTiP [56]. M.J.A.S. would like to thank the Humboldt Foundation for financial support. L.M.K.V. acknowledges support by an ERC Synergy grant (QC-Lab). J.I.C. acknowledges the ERC Advanced Grant QENOCOBA under the EU Horizon 2020 program (Grant Agreement No. 742102). Work in Innsbruck is supported by the ERC Synergy Grant UQUAM, the SFB FoQuS (FWF Project No. F4016-N23), and the Army Research Laboratory Center for Distributed Quantum Information via the project SciNet. Work at Harvard University was supported by NSF, Center for Ultracold Atoms, CIQM, Vannevar Bush Fellowship, AFOSR MURI and Max Planck Harvard Research Center for Quantum Optics.

M.J.A.S. and B.V. contributed equally to this work.

[1] C. Monroe, R. J. Schoelkopf, and M. D. Lukin, Sci. Am. 50 (2016).

[2] L. M. K. Vandersypen, H. Bluhm, J. S. Clarke, A. S. Dzurak, R. Ishihara, A. Morello, D. J. Reilly, L. R. Schreiber, and M. Veldhorst, npj Quantum Inf. **3**, 34 (2017).

[3] J. F. Poyatos, J. I. Cirac, and P. Zoller, Phys. Rev. Lett. **81**, 1322 (1998).

[4] K. Mølmer and A. Sørensen, Phys. Rev. Lett. **82**, 1835 (1999).

[5] G. J. Milburn, arXiv:quant-ph/9908037.

[6] J. J. García-Ripoll, P. Zoller, and J. I. Cirac, Phys. Rev. A **71**, 062309 (2005).

[7] A. Lemmer, A. Bermudez, and M. B. Plenio, New J. Phys. **15**, 083001 (2013).

[8] B. Royer, A. L. Grimsmo, N. Didier, and A. Blais, Quantum **1**, 11 (2017).

[9] M. J. A. Schuetz, G. Giedke, L. M. K. Vandersypen, and J. I. Cirac, Phys. Rev. A **95**, 052335 (2017).

[10] P. Rabl, S. J. Kolkowitz, F. H. L. Koppens, J. G. E. Harris, P. Zoller, and M. D. Lukin, Nat. Phys. **6**, 602 (2010).

[11] P. Scarlino, D. J. van Woerkom, U. C. Mendes, J. V. Koski, A. J. Landig, C. K. Andersen, S. Gasparinetti, C. Reichl, W. Wegscheider, K. Ensslin, T. Ihn, A. Blais, and A. Wallraff, arXiv:1806.10039.

[12] D. J. van Woerkom, P. Scarlino, J. H. Ungerer, C. Müller, J. V. Koski, A. J. Landig, C. Reichl, W. Wegscheider, T. Ihn, K. Ensslin, and A. Wallraff, Phys. Rev. X **8**, 041018 (2018).

[13] J. M. Gambetta, J. M. Chow, and M. Steffen, npj Quantum Inf. **3**, 2 (2017).

[14] J. Wendin, Rep. Prog. Phys. **80**, 106001 (2017).

[15] R. Hanson, L. P. Kouwenhoven, J. R. Petta, S. Tarucha, and L. M. K. Vandersypen, Rev. Mod. Phys. **79**, 1217 (2007).

[16] F. A. Zwanenburg, A. S. Dzurak, A. Morello, M. Y. Simmons, L. C. L. Hollenberg, G. Klimeck, S. Rogge, S. N. Coppersmith, and M. A. Eriksson, Rev. Mod. Phys. **85**, 961 (2013).

[17] From a technological point of view, this statement is important as thermal occupation of the resonator modes will be inevitable for reasonable temperatures when going to relatively long transmission lines (with correspondingly small fundamental mode frequencies). For example, for a (fundamental) mode frequency of $\sim$100 MHz the thermal occupation amounts to $\sim$20 thermal photons, even at very cold dilution fridge temperatures of $\sim$100 mK.

[18] T. E. Northup and R. Blatt, Nat Photonics **8**, 356 (2014).

[19] J. I. Cirac, P. Zoller, H. J. Kimble, and H. Mabuchi, Phys. Rev. Lett. **78**, 3221 (1997).

[20] B. Vermersch, P.-O. Guimond, H. Pichler, and P. Zoller, Phys. Rev. Lett. **118**, 133601 (2017).

[21] Z.-L. Xiang, M. Zhang, L. Jiang, and P. Rabl, Phys. Rev. X **7**, 011035 (2017).

[22] A. Das and B. K. Chakrabarti, Rev. Mod. Phys. **80**, 1061 (2008).

[23] E. Farhi, J. Goldstone, and S. Gutmann, arXiv:1411.4028.

[24] E. Farhi and Aram W. Harrow, arXiv:1602.07674.

[25] J. S. Otterbach, R. Manenti, N. Alidoust, A. Bestwick, M. Block, B. Bloom, S. Caldwell, N. Didier, E. S. Fried, S. Hong, P. Karalekas, C. B. Osborn, A. Papageorge, E. C. Peterson, G. Prawiroatmodjo, N. Rubin, C. A. Ryan, D. Scarabelli, M. Scheer, E. A. Sete *et al.*, arXiv:1712.05771.

[26] A. Kurcz, A. Bermudez, and J. J. García-Ripoll, Phys. Rev. Lett. **112**, 180405 (2014).

[27] M. Pino and J. J. García-Ripoll, New J. Phys. **20**, 113027 (2018).

[28] A. J. Kerman, New J. Phys. **15**, 123011 (2013).

[29] P.-M. Billangeon, J. S. Tsai, and Y. Nakamura, Phys. Rev. B **91**, 094517 (2015).

[30] N. Didier, J. Bourassa, and A. Blais, Phys. Rev. Lett. **115**, 203601 (2015).

[31] S. Richer and D. DiVincenzo, Phys. Rev. B **93**, 134501 (2016).

[32] L. Childress, A. S. Sørensen, and M. D. Lukin, Phys. Rev. A **69**, 042302 (2004).

[33] S. P. Harvey, C. G. L. Bøttcher, L. A. Orona, S. D. Bartlett, A. C. Doherty, and A. Yacoby, Phys. Rev. B **97**, 235409 (2018).

[34] P.-Q. Jin, M. Marthaler, A. Shnirman, and G. Schon, Phys. Rev. Lett. **108**, 190506 (2012).

[35] F. Beaudoin, D. Lachance-Quirion, W. A. Coish, and M. Pioro-Ladriere, Nanotechnology **27**, 464003 (2016).

[36] M. Russ and G. Burkard, J. Phys.: Condens. Matter **29**, 393001 (2017).

[37] Since our scheme (as opposed to schemes relying on transversal spin-resonator coupling) does not impose any (resonance) conditions on the qubit frequencies, the transition frequencies ω_i can be chosen sufficiently large (for example, for quantum dots the transition frequencies are largely tunable) such that thermal population of the qubits gets strongly suppressed.

[38] A. A. Houck, J. A. Schreier, B. R. Johnson, J. M. Chow, J. Koch, J. M. Gambetta, D. I. Schuster, L. Frunzio, M. H. Devoret, S. M. Girvin, and R. J. Schoelkopf, Phys. Rev. Lett. **101**, 080502 (2008).

[39] S. Filipp, M. Göppl, J. M. Fink, M. Baur, R. Bianchetti, L. Steffen, and A. Wallraff, Phys. Rev. A **83**, 063827 (2011).

[40] See Supplemental Material at http://link.aps.org/supplemental/10.1103/PhysRevB.99.241302 for further details.

[41] N. M. Sundaresan, Y. Liu, D. Sadri, L. J. Szőcs, D. L. Underwood, M. Malekakhlagh, H. E. Türeci, and A. A. Houck, Phys. Rev. X **5**, 021035 (2015).

[42] B. Peropadre, D. Zueco, D. Porras, and J. J. García-Ripoll, Phys. Rev. Lett. **111**, 243602 (2013).

[43] For example, for the two-qubit phase gate there is just a single eigenvalue $w_q = \pi/4$, such that $t_p = t_{\rm coh} = \pi/4J_{\rm max}$.

[44] We ignore single spin-relaxation processes, since the associated timescale T_1 is typically much longer than T_2. For example, for single-electron spins in silicon T_1 of up to $\sim$3 s has been demonstrated [45], while $T_2 \lesssim 10$ ms [47]. Still, if necessary, T_1 processes could be included along the lines of dephasing-induced errors [9].

[45] C. B. Simmons, J. R. Prance, B. J. Van Bael, T. S. Koh, Z. Shi, D. E. Savage, M. G. Lagally, R. Joynt, M. Friesen, S. N. Coppersmith, and M. A. Eriksson, Phys. Rev. Lett. **106**, 156804 (2011).

[46] M. Veldhorst, J. C. C. Hwang, C. H. Yang, A. W. Leenstra, B. de Ronde, J. P. Dehollain, J. T. Muhonen, F. E. Hudson, K. M. Itoh, A. Morello, and A. S. Dzurak, Nat. Nanotechnol. **9**, 981 (2014).

[47] M. Veldhorst, C. H. Yang, J. C. C. Hwang, W. Huang, J. P. Dehollain, J. T. Muhonen, S. Simmons, A. Laucht, F. E. Hudson, K. M. Itoh, A. Morello, and A. S. Dzurak, Nature (London) **526**, 410 (2015).

[48] R. Barends, J. J. A. Baselmans, S. J. C. Yates, J. R. Gao, J. N. Hovenier, and T. M. Klapwijk, Phys. Rev. Lett. **100**, 257002 (2008).

[49] A. Megrant, C. Neill, R. Barends, B. Chiaro, Y. Chen, L. Feigl, J. Kelly, E. Lucero, M. Mariantoni, P. J. J. O'Malley, D. Sank, A. Vainsencher, J. Wenner, T. C. White, Y. Yin, J. Zhao, C. J. Palmstrøm, John M. Martinis, and A. N. Cleland, Appl. Phys. Lett. **100**, 113510 (2012).

[50] A. Bruno, G. de Lange, S. Asaad, K. L. van der Enden, N. K. Langford, and L. DiCarlo, Appl. Phys. Lett. **106**, 182601 (2015).

[51] Consider (for example) fundamental frequencies of ∼100 MHz, as realized experimentally in Ref. [41], which translates to round-trip times of ∼10 ns. This timescale is much longer than state-of-the-art timing accuracies Δt of a few picoseconds as demonstrated experimentally in Refs. [52,53], leaving us with very small relative time jitter $(\omega_1/2\pi)\Delta t \sim 10^{-4}$.

[52] O. E. Dial, M. D. Shulman, S. P. Harvey, H. Bluhm, V. Umansky, and A. Yacoby, Phys. Rev. Lett. **110**, 146804 (2013).

[53] E. Bocquillon, V. Freulon, J. M. Berroir, P. Degiovanni, B. Plaçais, A. Cavanna, Y. Jin, and G. Fève, Science **339**, 1054 (2013).

[54] M. H. Michael, M. Silveri, R. T. Brierley, V. V Albert, J. Salmilehto, L. Jiang, and S. M. Girvin, Phys. Rev. X **6**, 031006 (2016).

[55] See http://itensor.org.

[56] J. R. Johansson, P. D. Nation, and F. Nori, Comput. Phys. Commun. **184**, 1234 (2013).